Acta Crystallographica Section D
Biological Crystallography
ISSN 0907-4449

The decameric structure of bovine pancreatic trypsin inhibitor (BPTI) crystallized from thiocyanate at 2.7 Å resolution

Cyril Hamiaux,[a] Thierry Prangé,[a,b]* Madeleine Riès-Kautt,[c] Arnaud Ducruix,[c] Sylvaine Lafont,[d]† Jean Pierre Astier[d] and Stéphane Veesler[d]

[a]Laboratoire pour l'Utilisation du Rayonnement Electromagnétique (LURE), Bâtiment 209d, Université Paris-Sud, 91405 Orsay CEDEX, France, [b]Laboratoire de Chimie Structurale, UFR-Biomédicale, rue M. Cachin, 93017 Bobigny CEDEX, France, [c]Laboratoire de Biologie Structurale (LEBS), Bâtiment 34, UMR 9920 CNRS, Campus du CNRS, 91198 Gif sur Yvette CEDEX, France, and [d]Centre de Recherche sur les Mécanismes de la Croissance Cristalline (CRMC2) CNRS, Campus de Luminy, Case 913, 13288 Marseille CEDEX 09, France

† Present address: LEBS-CNRS, 91198 Gif sur Yvette, France.

Correspondence e-mail: prange@lure.u-psud.fr

Received 24 March 1998
Accepted 22 June 1998

PDB Reference: bovine pancreatic trypsin inhibitor, 1bhc.

The structure of a monoclinic form of bovine pancreatic trypsin inhibitor (BPTI) crystallized from a thiocyanate solution has been determined and refined at 2.7 Å resolution. The space group is $P2_1$ with $a = 71.56$, $b = 73.83$, $c = 64.47$ Å, $\beta = 93.9^\circ$ and $Z = 20$. The ten independent molecules were located by a multi-body molecular-replacement search as developed in the *AMoRe* program, starting from a single monomer model (PDB code: 6PTI). The molecular arrangement of the subunits is a decamer resulting from the combination of two orthogonal fivefold and twofold non-crystallographic axes. This builds a globular micelle-like particle which minimizes hydrophobic interactions with the solvent. The refinement was conducted with non-crystallographic symmetry constraints up to a final residual of $R = 0.20$ ($R_{\rm free} = 0.26$). The root-mean-square deviations from ideal geometry were 0.015 Å and 1.6° on bond distances and bond angles, respectively. Several sites for thiocyanate ions were analyzed.

1. Introduction

In a general study of the influence of crystallizing agents for proteins, Riès-Kautt & Ducruix (1989, 1991) found that the thiocyanate anion can be effective at rather low concentration (~150 m*M*) in the crystallization of basic proteins. A number of known proteins were used as test cases, such as erabutoxin b, hen egg-white lysozyme (HEWL) or turkey egg-white lysozyme (TEWL).

The crystals obtained in these conditions are somewhat different from those obtained using 'classic' crystallizing agents such as sulfate or PEG agents. TEWL crystallizes as a monomer in a hexagonal form and diffracts to high resolution (1.65 Å: Howell, 1995; PDB code: 1TEW) while erabutoxin b crystallizes as a dimer with a slightly lower diffraction limit (1.7 Å, Saludjian *et al.*, 1992; PDB code 6EBX) than the monomeric form obtained from sulfate (1.45 Å, Smith *et al.*, 1988; PDB code 3EBX). *A priori*, the thiocyanate ion does not seem responsible for the new crystalline forms observed. They have occasionally been found under other circumstances: the hexagonal form of TEWL was previously obtained at pH 8.0 (Howell *et al.*, 1992; PDB code 3LZ2), as was the erabutoxin b dimer (Low, 1992).

The case of bovine pancreatic trypsin inhibitor (BPTI) illustrates the dramatic effect of thiocyanate. BPTI crystallized from phosphate is known to diffract at room temperature to very high resolution in three different orthorhombic cells (forms I to III plus a number of mutants; Table 1). The use of thiocyanate leads to a new monoclinic crystal form with unit-cell parameters $a = 71.56$, $b = 73.83$, $c = 64.47$ Å and $\beta = 93.9^\circ$. According to the estimated volume of the protein and a

Table 1
Crystallographic and NMR data for BPTI structures available in the Protein Data Bank (June 1998).

All X-ray structures are crystallized from phosphate solutions.

PDB code	Space group	Cell dimensions	Resolution (Å)	Conditions	*R* factor (%)	Reference
4PTI	$P2_12_12_1$	a = 43.10, b = 22.90, c = 48.60,	1.5	Native, form I	16.2	Marquart *et al.* (1983)
5PTI	$P2_12_12_1$	a = 74.10, b = 23.40, c = 28.90,	1.8/1	Native X-ray (form II)/ neutron	20/19.7	Wlodawer *et al.* (1984)
6PTI	$P2_12_12$	a = 55.20, b = 38.20, c = 24.05,	1.7	Native, form III	16.0	Wlodawer *et al.* (1987)
7PTI	$P2_12_12_1$	a = 74.36, b = 23.26, c = 28.88,	1.6	Double mutant (C30V, C51A)	17.0	Eigenbrot *et al.* (1990)
8PTI	$P4_22_12$	a = 46.75, b = 46.75, c = 50.61,	1.8	Mutant Y35G	15.9	Housset *et al.* (1991)
9PTI	$P2_12_12_1$	a = 74.44, b = 23.44, b = 28.85,	1.22	Oxidized M52	16.9	PDB entry 9PTI
1AAL	$C222_1$	a = 56.26, b = 29.58, c = 48.36,	1.6	Double mutant (C30V, C51A), 2 molecules in asymmetic unit	17.9	Eigenbrot *et al.* (1992)
1BPT	$P2_12_12_1$	a = 69.47, b = 23.35, b = 29.19,	2	Mutant Y23A	16.5	Danishefsky *et al.* (1993)
1BTI	$P2_12_12_1$	a = 69.12, b = 22.21, b = 28.71,	2.2	Mutant F22A	17.2	Danishefsky *et al.* (1993)
1NAG	$P2_12_12$	a = 55.72, b = 37.98, c = 23.79,	1.85	Mutant N43G	16.3	Danishefsky *et al.* (1993)
1FAN	$P2_12_12_1$	a = 69.31, b = 23.19, b = 29.24,	1.95	Mutant F45A	16.9	Danishefsky *et al.* (1993)
1BPI	$P2_12_12_1$	a = 75.39, b = 22.58, c = 28.60,	1.1	Native, 125 K, form II	14.9	Parkin *et al.* (1996)
1PIT	—	—	—	NMR structure	—	Berndt *et al.* (1992)

solvent content varying from 30 to 50%, the asymmetric unit can accommodate up to 12 independent molecules. The diffraction of this form extends only to a limit of 2.63 Å. The solubility of BPTI as a function of the chemical nature of the salt used as crystallizing agent follows the reverse Hofmeister series (Lafont, 1997) as previously described for HEWL (Riès-Kautt & Ducruix, 1989). Furthermore, the solubility of BPTI as a function of temperature may be reversed depending on the nature of the salt added to crystallize the BPTI, *i.e.* BPTI/SCN^- has a direct solubility while BPTI/Cl^- has an inverse one (*i.e.* less soluble at high temperature).

Veesler *et al.* (1996) and Lafont *et al.* (1997) have shown, using small-angle X-ray scattering (SAXS) and quasi-elastic light scattering (QELS) experiments, that during the nucleation process of BPTI using potassium thiocyanate as crystallizing agent the solution is monodispersed, but not monomeric, in the vicinity of the solubility curve. These experiments suggested a unique oligomeric particle to be formed prior to crystallization. The size of the particle was estimated to correspond to a tetramer (Lafont *et al.*, 1997; Lafont, 1997).

The aim of the present work is to determine the structure of the very uncommon multimeric form of BPTI crystallized from potassium thiocyanate, to determine if the thiocyanate anion plays a role in the aggregation state of the molecule and, finally, to study the specific intermolecular contacts in the packing which may have some biological relevance.

2. Materials and methods

2.1. Purification and crystallization

BPTI (Trasylol, batch no. 160591-121) was supplied by Bayer AG as a lyophilized powder. Previous studies on BPTI (Jolivalt *et al.*, 1997) showed that it contains 7%(*w*/*w*) chloride, corresponding to 13.8 molar equivalents. To prevent these chloride ions from having any effect on the crystallization process, the desalting protocol described by Riès-Kautt *et al.* (1994) was applied as follows. 100 mg of BPTI was dissolved in 5 ml of distilled water (pH 6.45). No initial dialysis was performed. The solution was mixed with a 1:1 mixture of cationic and anionic resins [15 ml of a cation-exchange resin (Biorad AG 50W-X8, H^+ form) and 15 ml of an anion-exchange resin (Biorad AG 1-X8, OH^- form)] for about 10 min in a 100 ml syringe. The protein solution was then recovered through a 0.2 µm filter. The resin was rinsed three times with 5 ml of water. The pH of the final solution was 10.1, close to the p*I* of

Table 2
Final data collection and reduction statistics.

Number of measured reflections	69959
Number of unique reflections	18308
Resolution limits (Å)	29.6–2.63
Redundancy	3.8
Data completeness (%)	85.5
Data completeness in the last resolution shell (2.63–2.71 Å) (%)	13.4
Overall $I/\sigma(I)$	11.1
$I/\sigma(I)$ for the last resolution shell (2.63–2.71 Å)	4.1
Overall $R_{\rm merge}$ (%)†	0.055
$R_{\rm merge}$ for data in the last resolution shell (2.63–2.71 Å) (%)	0.186

† $R_{\rm merge}$ is defined as $\sum_h \sum_i |\langle I(h)\rangle - I_i(h)| / \sum_h \sum_i I_i(h)$, where $I_i(h)$ is the ith observation of reflection h.

BPTI (pI = 10.5; Kassel, 1970). The desalted protein solution was then freeze-dried and kept at 253 K.

Crystals were grown at room temperature (291 K) using the seeding technique. 8 mg of BPTI was dissolved in 200 µl of a 250 mM KSCN solution prepared in a 50 mM sodium acetate buffer (pH 4.5). This solution corresponds to the metastable zone of the solubility diagram (Lafont *et al.*, 1997). A crystal seed was then added to the protein solution. Thin plate-like crystals (400 × 300 × 50 µm) grew within a few days. Some crystals grew to 2 mm in length. For data collection, crystals were mounted in quartz capillaries.

2.2. Data collection and processing

Data were collected from a single crystal using the rotation method at the DW32 synchrotron beam port at LURE, Orsay (Fourme *et al.*, 1992). Recordings were performed on a MAR Research image plate (180 mm diameter) at a wavelength λ = 0.97 Å, with crystal rotation $\Delta\omega = 2^\circ$, crystal-to-detector distance d = 230 mm, exposure time Δt = 60 s and temperature T = 283 K. The overall ω range covered was 180°. The crystals of BPTI/SCN$^-$ usually diffract to a maximum resolution of 2.63 Å.

Data processing was carried out using the *MOSFLM* program (Leslie, 1994), and data reduction and merging were performed with the *CCP*4 suite of programs (Collaborative Computational Project, Number 4, 1994). The cell parameters were refined using the post-refinement technique (Winkler *et al.*, 1979; Rossmann *et al.*, 1979) implemented in *MOSFLM*. The crystal belongs to the $P2_1$ space group, with unit-cell parameters a = 71.56, b = 73.83, c = 64.47 Å, β = 93.91°. The merged intensities were converted to structure-factor amplitudes by the method of French & Wilson (1978) and put on an quasi-absolute scale by a Wilson plot (Wilson, 1949) computed with data in the resolution range 4.5–2.7 Å. Results are summarized in Table 2.

2.3. Structure determination

In a search of non-crystallographic axes, the self-Patterson function was first investigated (program *POLARRFN*). The results are depicted as (φ, ψ) stereograms (Fig. 1) for two relevant sections of constant κ angle; these sections, given in polar coordinates for κ = 180 and 72°, show evidence for non-crystallographic symmetry elements (twofold and fivefold axes) in the cell. These two axes combine together to build a decamer structure.

The structure was solved by application of the *AMoRe* molecular-replacement program (Navaza, 1994) in its multi-body mode (Navaza *et al.*, 1993). The starting model was the monomer of BPTI form III (code 6PTI), solved at 1.7 Å resolution by Wlodawer *et al.* (1987). It includes 56 out of the 58 residues, as no density was found for the C-terminal Gly57 and Ala58. The water molecules and heteroatoms were removed from the initial model.

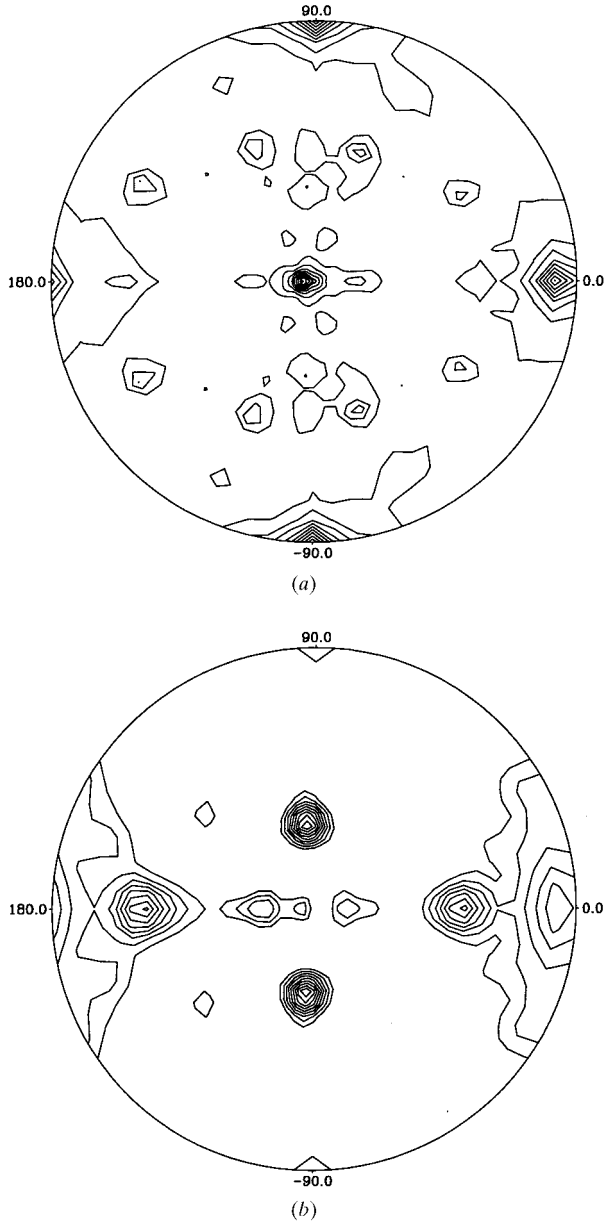

Figure 1
Self-rotation function (*POLARRFN*) for the two κ sections (*a*) 180° and (*b*) 72° (twofold and fivefold non-crystallographic axes, respectively). Maps calculated with all data. The crystallographic twofold axis ($\omega = \varphi$ = 90°) in κ section 180° is normalized to 100%. Contours are given at 10% intervals.

The structure was solved by successive steps within the 15–3 Å resolution limits using this model. A first run was performed in a search of five independent molecules. The first clearly contrasted solution proposed led to a correlation factor of 46.1% and an *R* factor of 43.5%. Graphic inspection of this solution using the *O* program (Jones *et al.*, 1991) revealed the five molecules spread in two groups: three on one side and two on the other. Within each group, there was no overlap between molecules. However, generating the symmetry-related molecules indicated that the model was still incomplete, as large void regions were present in the packing, thus confirming the results of the self-rotation function. The number of searched molecules was increased from six to ten using the same method, *i.e.* one model (monomer of form III) and ten positions to find. Correlation *C* and *R* factors for these different steps are shown in Table 3. We observed a gradual increase in the correlation factor, correlated with a decrease in the *R* factor and a progressive 'filling-in' of the void region in the packing of nine independent molecules. Direct calculation with ten independent molecules led to the previous determined nonamer plus the tenth molecule systematically superimposed onto a previously positioned molecule, leaving an empty cavity in the multimer. Instead, we used a more contrasted configuration by defining a two-body system: the previous nonamer plus a single tenth independent molecule. This permitted the location of the missing molecule in the top-ranked solutions. Finally, after replacing the molecules in the same asymmetric unit, the decamer was apparent (Fig. 2). A fast rigid-body refinement of the ten molecules was performed (Castellano *et al.*, 1992) using all data. The final correlation *C* and *R* factors are 62.4 and 37.2%, respectively (Table 3).

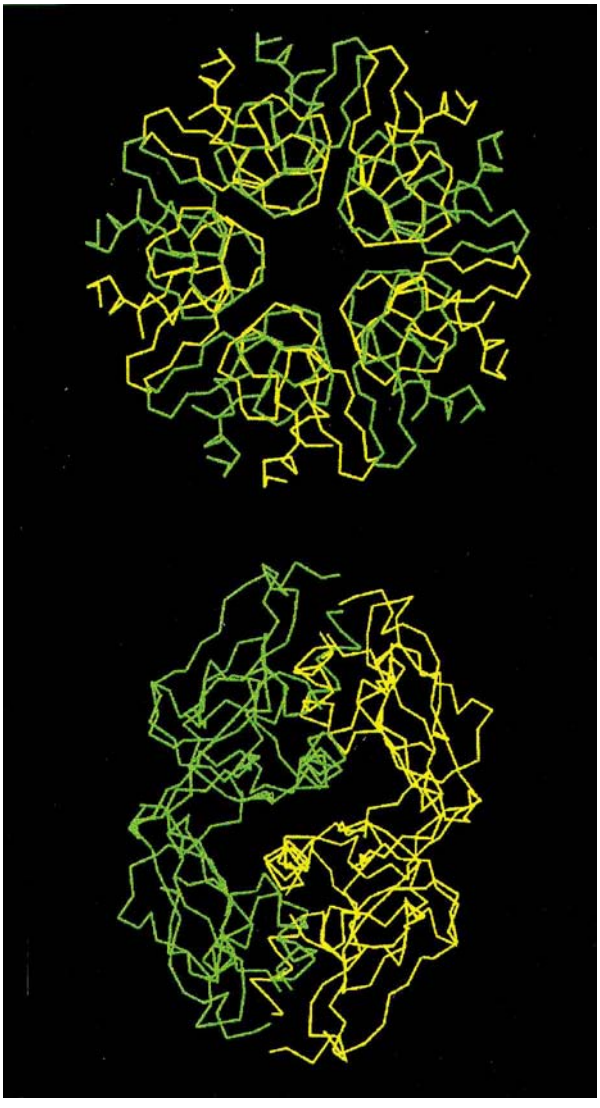

Figure 2
(*a*) View of the decamer along the fivefold non-crystallographic axis, Cα tracing only (colours are yellow and green for the two pentamers). (*b*) The same view rotated through 90° reveals the twofold non-crystallographic axis.

2.4. Refinement

The structure was refined using the *X-PLOR* molecular-dynamics program (Brünger, 1992). The starting point was the structure of the decamer originating from the rigid-body refinement. An isotropic *B* value of 15 Å^2 was assigned to all atoms and one position was kept for residues having alternate conformations with a full occupancy. According to the moderate resolution limit and the number of parameters to refine, the non-crystallographic symmetry information (NCS restraint as implemented in *X-PLOR*) was kept throughout the refinement process. In the first steps, the weight assigned to this restraint was relatively high ($W_{\rm NCS}$ = 300 kcal mol^{-1} Å^{-2}, 1 kcal = 4.184 kJ) in order to force the ten molecules to be identical. This was then gradually relaxed as the refinement progressed. The initial *R* factor was 40.9%. After several cycles of crystallographic/dynamic refinement in the 29–3 Å resolution range, the *R* factor converged to 29.4% ($R_{\rm free}$ = 31.9%). A grouped *B*-factor refinement was then performed without NCS (this combination of options is not available in *X-PLOR*), followed by an individual *B*-factor restrained refinement, using the NCS restraints again [the target deviation $\sigma(B_{\rm NCS})$ for the *B* factors was fixed at 1 Å^2]. During this run, the resolution shell was progressively increased to the practical range of 10–2.8 Å. At the end of this step, residuals were *R* = 24.2 and $R_{\rm free}$ = 27.8%. A graphic inspection of the structure revealed that (i) two residues (Lys46 and Glu49) in all the molecules had to be rebuilt and (ii) there were numerous round-shaped peaks in the vicinity of many polar atoms of the model. A small number of them, with electron density above 7σ, were considered as putative sites for the expected thiocyanate ions. However, no attempt to directly interpret these peaks as S atoms was performed at this stage. Despite the moderate resolution of the map, water location was attempted (programs *PEAKMAX* and *WATPEAK* from *CCP*4, followed by graphic inspection with the *O* program). Water molecules were considered part of the model when meeting both density and geometry criteria: a density above the 3σ level of the average density of the $|F_o| - |F_c|$ map and a distance within the 2.5–3.8 Å range from a polar atom. 190 water molecules, with an initial *B* factor of 30 Å^2, were included in the model. No NCS symmetry was applied to

Table 3
Molecular replacement: progress in the figures of merit as a function of the number of independent subunits used in the calculations.

Rotations/translations are given with respect to a model with origin at the centre of mass and placed in its 'minimum cell'.

Number of subunits	Corr†	R‡	Position number	α (°)	β (°)	γ (°)	T_x (Å)	T_y (Å)	T_z (Å)
5	46.1	43.5	1	254.6	29.6	112.6	20.4	−3.6	24.5
			2	92.1	43.9	235.8	38.5	22.5	18.3
			3	253.2	39.7	183.7	39.7	10.9	36.2
			4	264.2	44.3	247.5	28.4	30.9	50.0
			5	82.0	37.7	172.5	29.1	42.5	3.2
6	52.1	41.4	6	88.6	28.3	96.3	50.0	57.0	−5.7
7	55.9	39.7	7	276.6	38.5	309.3	1.7	29.2	46.6
8	60.3	37.8	8	276.4	29.5	21.3	−3.4	7.4	31.3
9	63.4	36.6	9	105.7	39.7	296.6	65.2	24.1	18.6
10	62.4	37.2	nonamer	0.5	172.2	180.5	−1.9	22.4	27.3
			monomer	274.7	28.9	23.0	−3.4	13.8	31.0

† The correlation coefficient is calculated as $\mathrm{Corr} = [\sum_h(|F_{obs}|^2 - |\overline{F_{obs}}|^2)(|F_{calc}|^2 - |\overline{F_{calc}}|^2)]/\{[\sum_h(|F_{obs}|^2 - |\overline{F_{obs}}|^2)^2 \sum_h(|F_{calc}|^2 - |\overline{F_{calc}}|^2)^2]^{1/2}\}$. ‡ The R factor is calculated as $R = \sum_h(||F_{obs}| - |F_{calc}||)/\sum_h |F_{obs}|$.

the water molecules. Further cycles of refinement led to R = 22.1% and R_{free} = 27.0%. At this stage, the NCS weighting scheme was modified to give side chains more freedom than the main chain [W_{NCS} = 150 and 75 kcal mol^{-1} Å^{-2}, $\sigma(B_{NCS})$ = 2 and 3 Å^2 for main and side chains, respectively]. Despite the limited resolution of 2.8 Å, the quality of the map was good enough to reveal, in all ten molecules, a bifurcated density for residue Met52 that was best modelled by giving this residue two alternate conformations (fixed as half-weighted occupancies). In the last cycle of refinement, the side chains of all Met52 residues were allowed a relaxed NCS weighting scheme with W_{NCS} = 10 kcal mol^{-1} Å^{-2} and $\sigma(B_{NCS})$ = 3 Å^2. Data resolution was extended to the maximum of 2.7 Å. 28 more water molecules were inserted into the model at this stage. After a final graphic inspection, only 132 water molecules whose corresponding electron density was more than 2σ in the $2|F_o| - |F_c|$ map were kept in the model. Finally, side chains for which non-crystallographic equivalence was obvious for packing reasons (Arg1, Glu3, Lys15, Lys26 and Arg39) were removed from the NCS restraint weighting scheme. At this stage, the model includes ten BPTI molecules and 132 water molecules with R = 20.0% and R_{free} = 26.0%.

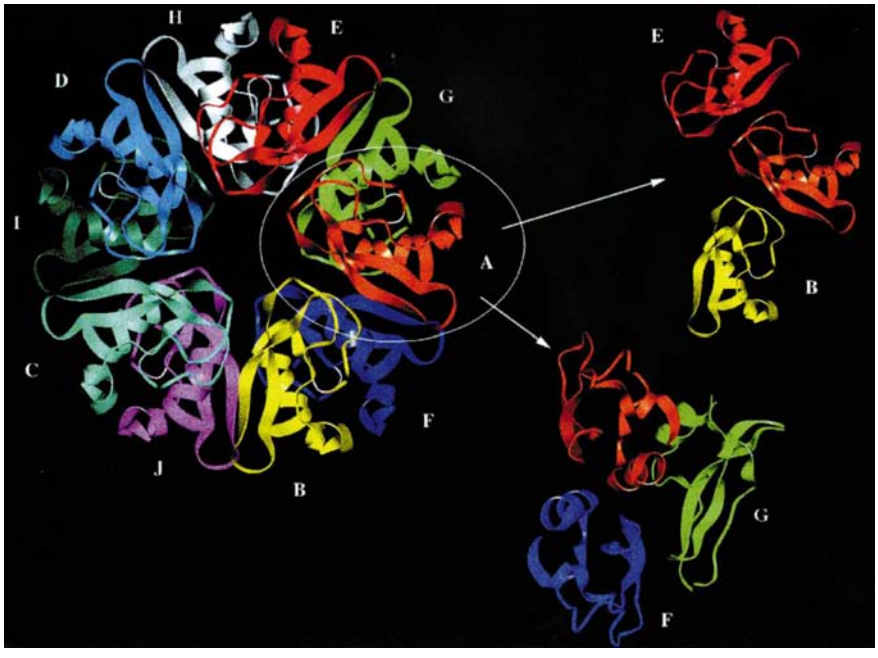

Figure 3
The contacts around a single BPTI molecule. A isolated molecule A (in orange) has contacts with four neighbours: two within the pentamer (A/B and A/E) and two with molecules belonging to the other pentamer (A/F and A/G). The larger contact area is A/G, which is twice as large as the others. Interactions are mediated by helix–helix and helix–β-sheet contacts at the C-termini (S—S bridges not reported).

2.5. Searching for thiocyanate ions

As stated above, a number of peaks with unexpectedly high electron density were systematically refined as water molecules. As a consequence, their B factor converged to values far below a threshold fixed as the average $\langle B \rangle$ of the Cα chain (23 Å^2) or, in some cases, to negative values. A final omit map was calculated by removing all the solvent molecules. The strong peaks above 5σ were assumed to be S atoms of thiocyanate ions. They were further analysed in terms of shape and contacts with the neighbouring positively charged residues according to Tchertanov & Pascard (1997). Among them, 14 showed characteristic elongated densities that could be plausible locations for SCN^- ions. After introducing these thiocyanates into the model, additional cycles of refinement were performed. A subsequent improvement of the map was observed in some regions, but there was only a limited improvement in the residuals. The sulfur temperature factors were finally checked against an omit map calculated by excluding these thiocyanates, plus a single S atom from a disulfide bridge for scaling. Ten thiocyanates survived and were kept in the final model. The four others, showing only isotropic electron density, were found at the same locations as structural waters already observed in the high-resolution structures (W111 to W113 in 4PTI, 5PTI and 6PTI) and were kept as single well ordered O atoms. This finally leads to a total number of 118 water molecules.

Table 4
Final statistics at the end of the refinement.

Final parameters

Resolution range (Å)	10–2.7
Number of reflections with $F \geq 2\sigma(F)$	17807
Number of protein atoms	4490
Number of water molecules	118
Number of thiocyanates	10
Overall average $\langle B \rangle$ values (Å^2)	
Main-chain atoms	22.9
Side-chain atoms	27.8
Solvent molecules	32.1
Thiocyanate ions	45.2
R.m.s. bond lengths (Å)	0.015
R.m.s. bond angle (°)	1.6
R factor	20.1
$R_{\rm free}$	26.5

Average $\langle B \rangle$ values by subunit (Å^2)

Subunit	Pentamer	Main chain	Side chain
A	1	17.9	22.1
B	1	18.0	22.8
C	1	20.4	23.8
D	1	30.5	36.1
E	1	30.7	36.9
F	2	17.2	22.1
G	2	20.7	24.9
H	2	30.2	35.7
I	2	27.8	34.4
J	2	16.3	20.4

The final parameters for the BPTI decamer model after completion of refinement are given in Table 4. Atomic coordinates and structure factors have been deposited with the Protein Data Bank (Bernstein *et al.*, 1977).

3. Results and discussion

BPTI is a small rigid protein of 58 residues. The structure consists of a double-stranded antiparallel β-sheet (residues 16–36) maintained by three disulfide bridges. A short helix is present at the C terminus. The rigidity of the structure explains the high resolution of the monomeric forms already published (forms I, II and III are available in the Protein Data Bank, plus a number of mutants; see Table 1). The solvent content of the monomeric crystals is very low, in the range 36–38%, with an average volume of about 8200 Å^3 for the BPTI molecule. In the case of the decamer, the higher solvent content (52%), together with structural variations between subunits within the decamer, is probably responsible for the lower resolution observed.

3.1. Building the decamer

The molecular-replacement procedure did not directly provide the assembly of the decamer in the asymmetric unit. The ten molecules, though correctly oriented and translated, were spread in the cell without evident non-crystallographic symmetry relationships. Building the correct asymmetric unit is not an easy task, but is simplified using the concept of maximizing the protein–protein contacts in the multimer (Janin & Rodier, 1995) by calculating either a pairwise area of contact or a common van der Waals surface. To tackle the case of ten molecules, a small program was designed to calculate the interactions between a pair of molecules (one moving and one fixed: the target) which maximizes the criterion $R_v = \sum_i \sum_j s_{ij}$, where i and j are the summation indexes for the moving and the target molecule, respectively, and s_{ij} is the van der Waals surface of contact if the interatomic distance d_{ij} falls within the 2.5–4 Å range, or zero otherwise. To the moving molecule are applied all the symmetry operations of the space group, plus translations along the three axes, in order to bring the moving molecule into the vicinity of the target. The oriented/translated molecule giving the highest R_v parameter was fixed and added to the target. This process is repeated for all the remaining molecules. The result is a multimer which maximizes internal contacts. This automated brute-force method has the advantage of being quite fast. The same result was obtained using an explicit calculation of the contact surface. The final asymmetric unit is shown in Fig. 2.

3.2. The final model

The average positional errors in the coordinates of the decamer are estimated from a Luzzati plot of the R factor against d^* (Luzzati, 1952) to be 0.25–0.3 Å.

Least-squares superimposition of all the subunits was performed (Fig. 5). R.m.s. deviations between subunits are in the ranges 0.05–0.1 and 0.2–0.4 Å for main chains and side chains, respectively. Calculated against the monomeric forms of BPTI (forms II and III) these values fall between 0.4–0.6 and 1.5–1.8 Å, respectively.

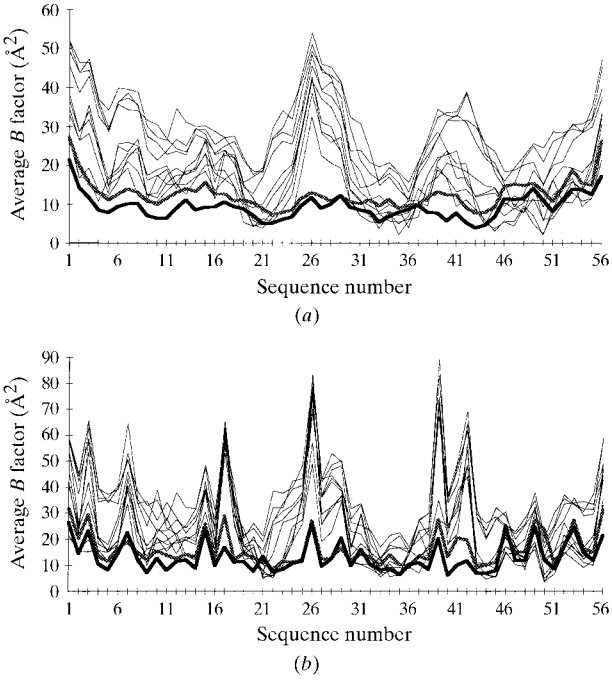

Figure 4
Analyses of B factors with sequence number. (*a*) Main-chain and (*b*) side-chain diagrams show the ten subunits (light tracing) superimposed with forms II (dashed tracing) and III (bold tracing).

The torsion angles (φ, ψ) of the main chain were calculated according to Ramakrishnan & Ramachandran (1965). No residue falls in the disallowed region of the corresponding energy diagram.

Several residues were associated with weak densities in the $2|F_o| - |Fc|$ map. This is not surprising, as BPTI structures with much better resolution limits had previously shown some disordered residues [crystal form II, at 1.22 Å resolution, was modelled with eight alternative conformations for residues Asp3, Glu7, Arg39, Arg42, Glu49, Asp50, Met52 and Arg53 (9PTI); crystal form III, at 1.7 Å resolution, was modelled with two alternate conformations for Arg39 and Asp50 (6PTI; Wlodawer *et al.*, 1987)]. In the decamer, no alternative conformation, except for Met52, has been found for other residues. In addition, a small number of disordered residue side chains showed no density at all. They were, however, kept in the refinement with full occupancy factors, letting their B factors reach extremely high values (up to 90 Å^2). They correspond mostly to loop regions. Nevertheless, in some subunits, when these residues are in contact with symmetry-related ones, they display well defined electron densities and B factors close to the average protein $\langle B \rangle$ value. The temperature factors of the refined model are reported in Fig. 4 as a function of the chain sequence. The light curves represent the $\langle B \rangle$ factors for each of the ten subunits. Superimposed on these plots are the same B curves obtained from the monomeric forms II and III of BPTI. This shows equivalence in the disordered residues (as long as no specific packing contacts are involved) in all the subunits. One can also note the equivalence between the high-resolution curve of 6PTI and those of the decamer, expanded by a factor of 3–4.

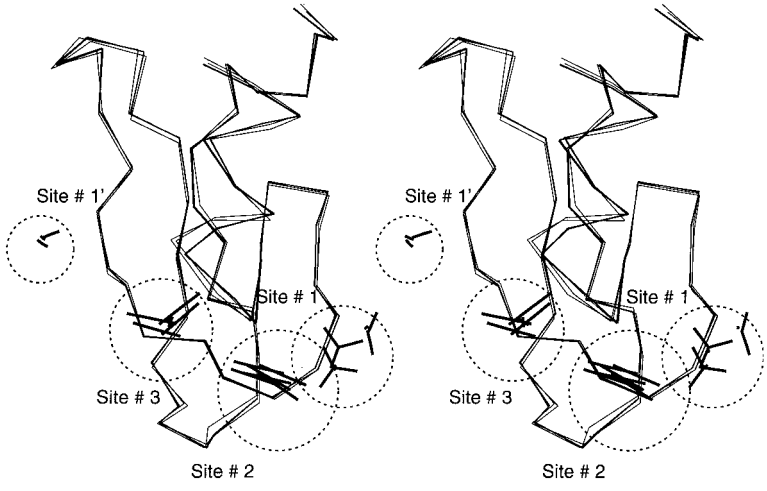

Figure 5
Least-squares fit of Cα chains of the ten subunits of the decamer, plus the three structures 4PTI, 5PTI and 6PTI crystallized in phosphate. The locations of the binding zones of thiocyanates are indicated by dashed circles with respect to this common target molecule. The two phosphate anions of 5PTI and 6PTI structures are also reported – they correspond to the anionic site 1. Due to non-crystallographic symmetry considerations, the three anionic sites correspond to four different binding zones. Site 1 and site 1′ are equivalent within each pentamer (molecules SCN1–SCN3) *e.g.* thiocyanate-labelled SCN1 lies in site 1 for subunit G and in site 1′ for subunit F. Site 3 (SCN4–SCN7) is in the vicinity of residues 47–49 of dimers A/F, B/J, C/I and E/G, while site 4 (SCN8–SCN10) connects pairs of Lys46 from two different pentamers: D/I, B/F and H/E.

3.3. A dimer of pentamers or a pentamer of dimers?

Within the multimer, each subunit displays interactions with four neighbours: two major surfaces of contact ($s_1 \simeq 460$, $s_2 \simeq 430$ Å^2) and two of lesser importance ($s \simeq 220$ Å^2). At first sight, the subunits are assembled as two plate-shaped pentamers (Fig. 2, 3) associated by their convex faces. Thus, a single nth isolated molecule in a pentamer ring has contacts on both sides with the previous [$(n-1)$th] and the next [$(n+1)$th] molecule in the pentamer ring, plus contacts with two subunits belonging to the other pentamer. However, inter-pentamer contacts (*e.g.* A/F and A/G), are more important than the intra-pentamer contacts (A/B and A/E). Hence, the multimer may alternatively be considered as a pentamer of dimers instead of a dimer of pentamers. One possible dimer association (*e.g.* A/G) is built through mutual helix–loop/loop–helix contacts at the C-termini involving residues 42–52. Indeed, there are a number of additional contacts mediated by water molecules but not present in all of the subunits. Table 5 summarizes the main protein–protein contacts observed around an isolated subunit of the decamer. Most of these contacts are common to the nine other subunits of the multimer.

3.4. Intermolecular contacts between decamers

Conversely, fewer contacts are observed between the different decamers which form perfect globular objects in the packing (Table 6). However, some subunits are more or less tightly fixed within the decamer, and their loose contacts may explain why four monomers have an average $\langle B \rangle$ value much higher than the others: $\langle B \rangle$ is about 35 Å^2 for monomers D, E, H and I, which correlates with no inter-decamer contacts for subunits D and E, while H and I have only weak packing contacts.

Finally, if the monomer itself has a very rigid structure, stabilized by more than 150 internal contacts, the whole decamer is constructed using only a total of 155 polar contacts. On a larger scale, the number of contacts forming the crystal is only ~21 polar contacts per decamer with symmetric equivalents in the cell. This leads to very weak crystal packing, which correlates with the low resolution and the weak mechanical and thermal stabilities observed for the crystals.

3.5. The hydration of the decamer

BPTI structures at a resolution of better than 1.2 Å are prototypes of a well ordered hydration network. It shows fused pentagon and hexagon rings bonded either to the protein or to other water molecules. The geometry of the network has been described in great detail by Wlodawer *et al.* (1987) and, at low temperature, by Parkin *et al.* (1996). At a resolution of 2.7 Å it would be speculative to discuss the rather poorly defined hydration network of the decamer. However, four internal waters are present at equivalent sites in six subunits. These molecules

are present in all the high-resolution structures and were also observed by NMR in solution (Otting & Wütrich, 1989). These internal waters have been described as 'an integral part of the structure' (Fig. 6*b*). In the other four subunits, the corresponding sites are only partially occupied but still remain visible. In contrast to the rest of the structure, these buried water molecules have *B* factors in the range 10–15 Å^2, far below the average $\langle B \rangle$ of the protein.

3.6. The thiocyanate ions and their role in decamer building

Thiocyanate anions have been found to be very effective in the crystallization of hen or turkey egg-white lysozymes (HEWL, TEWL) and other basic proteins (Riès-Kautt & Ducruix, 1989, 1991). More recently, small-angle X-ray scattering analysis of under-saturated solutions showed that the presence of salt in solution tends to modify protein–protein interactions from repulsive to attractive (Ducruix *et al.*, 1996; Veesler *et al.*, 1996). The efficiency of anions in inducing this modification was found to be the same as their efficiency in crystallizing basic proteins, *i.e.* it follows the reverse order of the Hofmeister series. As far as thiocyanate ion is concerned, a binding process to basic side chains of the protein in solution which induces crystallization was proposed (Riès-Kautt & Ducruix, 1991). This hypothesis was in agreement with two structure determinations: erabutoxin b, solved at 1.7 Å resolution (Saludjian *et al.*, 1992), and the hexagonal form of turkey egg-white lysozyme (TEWL), determined at 1.65 Å resolution (Howell, 1995). Both structures contain complexed thiocyanate ions. In erabutoxin b, the thiocyanate lies between two molecules and a dimeric association through an intermolecular antiparallel β-sheet is built. The thiocyanate ion is located in a polar cave at the interface of the dimer, with the N atom interacting with side chains of Arg33A (3.26 Å) and Ser23B (2.68 Å) and the S atom forming contacts with the carbonyl O atom of Cys54B (3.31 Å) and a water molecule (3.43 Å). In TEWL, no dimer is observed and the thiocyanate sits close to the interface of two symmetry-related molecules. In this case, there are no strong electrostatic interactions for the N atom and, instead, the S atom interacts directly with

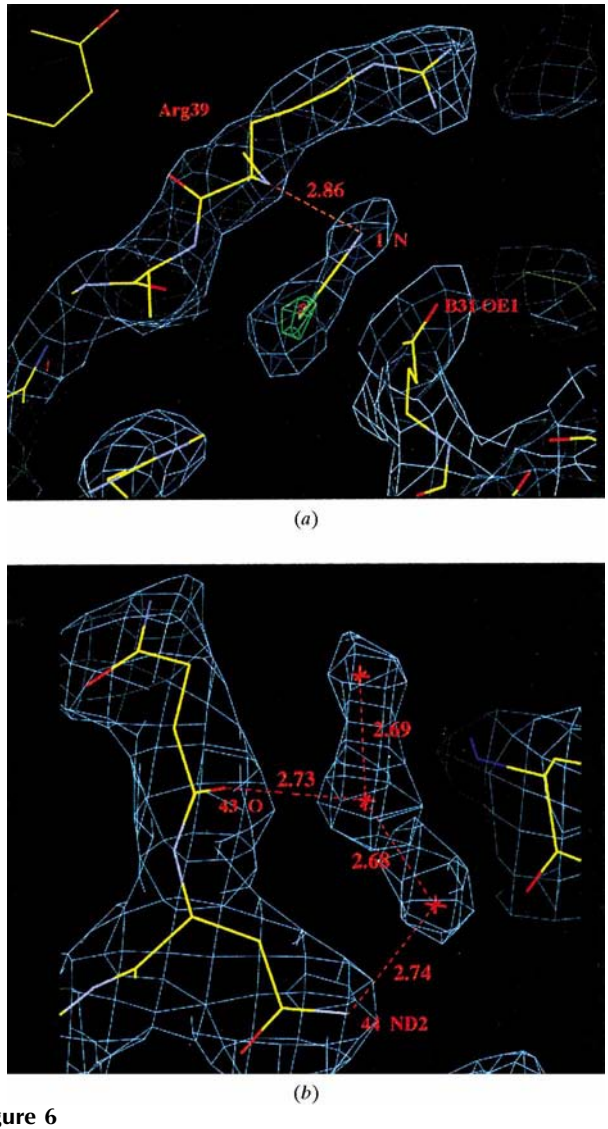

Figure 6
Two characteristic parts of the $2F_o - F_c$ electron-density map (contouring: 1.5σ above the mean, with calculated phases). (*a*) One of the thiocyanate ions, located in site 1. The N atom of the thiocyanate is connected to Arg39D N (d = 2.90 Å) and also to Thr32B O (d = 2.74 Å). The S atom is close to Ala40D N (d = 3.47 Å) and Thr32B OG1 (d = 3.26 Å). (*b*) The internal water molecules in subunit B. These waters (labelled w111 to w113 in the high-resolution structures 4PTI, 5PTI and 6PTI) are an integral part of the BPTI structure and are visible in most of the subunits at the resolution of 2.7 Å.

Table 5
Contacts between a reference subunit (molecule A) and all others within the decamer (molecules B to J).

These contacts are, within a given r.m.s. range, present in all the other subunits numbered in a circular fashion. The numbering is given in Fig. 3 (pentamer 1: A to E; pentamer 2: F to J).

Atom in molecule A	Molecule	Atom	Distance (Å)
Phe33 N	B†	Gly37 O	3.39
Thr32 OG1	B†	Gly37 O	3.07
Thr32 OG1	B†	Tyr35 OH	2.94
Gly37 O	E†	Phe33 N	3.46
Gly37 O	E†	Thr32 OG1	2.94
Tyr35 OH	E†	Thr32 OG1	2.94
Glu49 OE2	F	Tyr21 OH	2.87
Tyr21 OH	F	Glu49 OE2	2.62
Arg42 NH2	G	Arg53 O	3.61
Arg42 NE	G	Arg53 O	3.67
Asn44 OD1	G	Arg53 NH2	3.37
Asn44 O	G	Arg53 NH2	2.44
Lys46 N	G	Asp50 OD1	2.82
Lys46 N	G	Asp50 OD2	3.35
Ser47 N	G	Asp50 OD2	3.24
Glu49 OE2	G	Arg20 NH1	2.57
Glu49 OE1	G	Arg20 NH1	2.45
Asp50 OD2	G	Asp50 OD2	2.51
Asp50 OD2	G	Ser47 N	3.30
Asp50 OD2	G	Lys46 N	3.45
Asp50OD1	G	Lys46 N	2.87
Arg53 NH2	G	Asn44 O	2.42
Arg53 NH2	G	Asn44 OD1	3.40
Arg53 O	G	Arg42 NE	3.39
Arg53 O	G	Arg42 NH2	3.43
Arg20 NH1	G	Glu49 OE1	2.52
Arg20 NH1	G	Glu49 OE2	2.70

† Belong to the same pentamer.

Table 6
Intermolecular contacts between the decamers in the cell.

First atom		Second atom		
Symmetry operator†	Atom	Symmetry operator†	Atom	Distance (Å)
A (1 0 0 0)	Asp3 OD1	C (2 1 0 0)	Arg39 NH2	3.56
	Asp3 OD1	C (2 1 0 0)	Arg39 NH1	3.61
	Asp3 OD2	C (2 1 0 0)	Arg39 NH2	3.71
	Lys26 NZ	C (2 1 0 0)	Gly12 O	3.70
B (1 0 0 0)	Tyr10 OH	G (2 1 −1 0)	Asp3 OD1	3.42
	Lys41 NZ	G (2 1 −1 0)	Asp3 OD2	3.49
	Lys41 NZ	G (2 1 −1 0)	Asp3 OD1	3.19
C (1 0 0 0)	Asp3 OD2	F (2 1 −1 −1)	Lys41 NZ	3.30
	Arg39 NH2	A (2 1 −1 0)	Asp3 OD1	3.56
	Arg39 NH2	A (2 1 −1 0)	Asp3 OD2	3.71
	Arg39 NH1	A (2 1 −1 0)	Asp3 OD1	3.61
	Gly12 O	A (2 1 −1 0)	Lys26 NZ	3.70
D (1 0 0 0)	—	—	—	—
E (1 0 0 0)	—	—	—	—
F (1 0 0 0)	Lys41 NZ	C (2 1 0 −1)	Asp3 OD2	3.30
G (1 0 0 0)	Asp3 OD2	B (2 1 0 0)	Lys41 NZ	3.19
	Asp3 OD1	B (2 1 0 0)	Lys41 NZ	3.49
	Asp3 OD1	B (2 1 0 0)	Tyr10 OH	3.42
	Arg39 NH2	J (2 1 0 −1)	Asp3 OD1	3.36
	Arg39 NH2	J (2 1 0 −1)	Asp3 OD2	3.66
	Arg39 NH1	J (2 1 0 −1)	Asp3 OD1	3.50
H (1 0 0 0)	Tyr10 OH1	I (2 0 0 −1)	Asp3 OD1	3.48
	Asp3 OD1	I (2 0 0 −1)	Lys26 NZ	3.63
I (1 0 0 0)	Asp3 OD1	H (2 0 −1 −1)	Tyr10 OH	3.48
	Lys26 NZ	H (2 0 −1 −1)	Asp3 OD1	3.63
J (1 0 0 0)	Asp3 OD1	G (2 1 −1 −1)	Arg39 NH2	3.36
	Asp3 OD1	G (2 1 −1 −1)	Arg39 NH1	3.50
	Asp3 OD1	G (2 1 −1 −1)	Arg39 NH2	3.66

† The symmetry operators are given in parentheses: the first number refers to the symmetry operation of the space group (*International Tables for X-ray Crystallography*) and the three others are the translations along the axes. The prefix letter is the subunit code within the decamer.

Arg14 NH2 (3.28 Å), Arg14 NE (3.42 Å) and a water molecule (3.57 Å). In these two structures, the binding mode of thiocyanate is reversed.

In the decamer of BPTI, only a small number of thiocyanates show the characteristic elongated signature previously observed in the high-resolution electron-density maps of erabutoxin b and TEWL. The shapes of some thiocyanates were found to correspond equally well to two discrete water molecules. If these thiocyanate ions are real, they would certainly be either strongly disordered or difficult to characterize, owing to the limited resolution of the crystals. From all the putative sites, ten were accepted as possible thiocyanates.

These ten molecules are distributed in three zones. The major anionic site (Fig. 6*a*) is in the vicinity of Arg39 side chain, and is present at equivalent locations in subunits C, D and E. This main site corresponds to the anionic site of phosphate anions observed in the high-resolution structures 5PTI and 6PTI. The other sites are mostly in the vicinity of lysine side chains (*e.g.* Lys46) which point inwards towards the central channel built by the fivefold non-crystallographic symmetry (Fig. 5).

In solution, salt-effect studies on BPTI have been extensively carried out by NMR (Modi *et al.*, 1989*a*,*b*; Christoffersen *et al.*, 1996; Böckmann & Guittet, 1995; Jolivalt *et al.*, 1998). Interactions of proteins with solvents may be described as a two-component reaction: a direct ion binding to the protein and a modification of the electrostatic potential (screening or swamping effects). The first mechanism is usually related to the biological function of the protein and may be interpreted as a thermodynamic equilibrium between discrete complexed and uncomplexed species. The second mechanism is more complex and proceeds *via* partial neutralization of the polar side chains at the protein surface.

Jolivalt *et al.* (1998) observed both a specific binding of thiocyanate and a modification of the BPTI electrostatic potential, as deduced from chemical-shift and relaxation-time measurements. The larger local effect was found to affect the amide proton of Arg42 and was interpreted as specific binding of a thiocyanate with a dissociation constant $K \simeq 90$ mM. Despite this low affinity constant, the authors clearly confirm a dramatic influence of thiocyanate on the molecule. It is also interesting to note the crystallographic site of thiocyanate in the decamer is Arg39 (Fig. 6*a*) which lies in the same region as Arg42.

In another series of experiments, Lafont *et al.* (1997) and Veesler *et al.* (1996) investigated small-angle X-ray scattering experiments near the nucleation point ($\sim$30–40 mg ml^{-1}). They confirmed that anions, and particularly thiocyanate, reverse the repulsive effect, leading to the formation of aggregates with a hydrodynamic radius roughly compatible with a tetramer. However, no oligomeric model was available at that time to refine these conclusions. From reinvestigation of the light-scattering profiles at small X-ray angles using the model determined in the present study, a more complex situation is likely to exist: neither the full decamer nor part of it (tetramer, pentamer *etc.*) are able to model accurately the state of BPTI at high thiocyanate concentration. A fast dynamic exchange between several species is probably the best description of what is observed.

The rather low affinity of thiocyanate to BPTI, as deduced from NMR experiments, is not a unique example. Most interactions of mineral anions such as chloride, nitrate (Galanter & Labotka, 1991) or thiocyanate (Modi *et al.*, 1989*b*; Crull & Goff, 1993) are of the same order of magnitude in a number of different proteins. Again, these studies support the observation that, even though thiocyanate is a particular polarizable soft agent, it does not differ from others anions: in the particular case of BPTI, we have observed that sodium chloride is also able to form pentamers of BPTI in crystals,

though in a different crystal form and at a different concentration (Hamiaux, 1998).

The formation of the globular decamer depicted in Fig. 7 is a good illustration of how the total energy of the system can be minimized upon increasing the relative concentration of negatively charged ions to BPTI. The orientation of the molecules, with their positively charged residues pointing outwards and hydrophobic parts inwards, is likely to be the driving force responsible for the attractive effect observed in solution. The efficiency of the association can be appreciated from surface calculations in the crystal: a single isolated BPTI molecule with an accessible area of 1165 Å^2 exposes less than half of this area when included in the final multimer. Most of the positively charged residues (Lys15, Lys26, Lys41, Arg1, Arg17, Arg39, Arg42 and Arg53) are still accessible to the solvent.

4. Concluding remarks

In the presence of potassium thiocyanate, an unusual multimeric form of BPTI is obtained. Ten independent molecules were successfully located by molecular replacement starting from a single BPTI model molecule. The analysis of contacts between the subunits of the particle shows that the decamer is formed by combination of a fivefold and a twofold non-crystallographic symmetry axis with a high degree of accuracy. Previous studies in solution, by small-angle X-ray scattering and quasi-elastic light scattering (SAXS and QELS) in the vicinity of the crystallization point, were in favour of the construction of a discrete multimer in solution. The oligomerization of the particle was initially estimated from its scattering coefficient to be a tetramer, and the crystal, once formed, was expected to retain this association in the packing. The present structural analysis gives additional elements justifying a pre-aggregation state of the protein prior to crystallization, though the real state of this particle in solution remains still unclear. Once the crystal is formed, the result is the formation of a globular decamer.

This structure represents the third complex of a protein crystallized in presence of thiocyanate. The two others are at a higher resolution than the one reported here: erabutoxin b dimer diffracts to 1.7 Å and turkey egg-white lysozyme to 1.65 Å. In these two structures, thiocyanate ions were unambiguously identified in the packing with contacts toward arginine residues, though differently positioned and complexed. Despite the lower resolution of the decamer (2.7 Å), it is still possible to interpret some of the residual electron densities as plausible sites for thiocyanate ions. Ten of them were retained in the final refined model.

In the case of erabutoxin b and lysozyme, the same crystal forms were previously obtained at basic pH without the aid of thiocyanate. This would suggest that, at acidic pH, thiocyanate ion stabilizes the crystalline forms normally obtained under basic conditions. However, the fact that all three structures contain thiocyanate signatures between the subunits is in favour of an active role for the SCN^- anion in building the crystal.

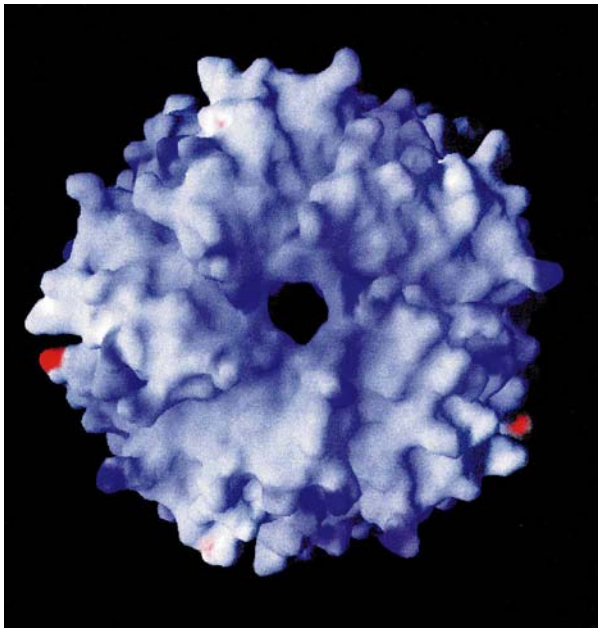

Figure 7
The surface of the BPTI decamer: the particle adopts a micellar structure with most of the positively charged residues pointing outwards and hydrophobic residues turned inside.

References

Berndt, K. D., Guntert, P., Orbons, L. P. & Wüthrich, K. (1992). *J. Mol. Biol.* **227**, 757–775.

Bernstein, F. C., Koetzle, T. F., Williams, J. B., Meyer, E. F. Jr, Brice, M. D., Rodgers, J. R., Kennard, O., Shimanouchi, T. & Tasumi, M. (1977). *J. Mol. Biol.* **112**, 535–542.

Böckmann, A. & Guittet, E. (1995). *J. Chim. Phys. Phys. Chim. Biol.* **92**, 1923–1928.

Brünger, A. (1992). *X-PLOR Manual, Version 3.0.* Yale University, New Haven, CT, USA.

Castellano, E. E., Oliva, G. & Navaza, J. (1992). *J. Appl. Cryst.* **25**, 281–284.

Christoffersen, M., Bolvig, S. & Tüchsen, E. (1996). *Biochemistry*, **35**, 2309–2315.

Collaborative Computational Project, Number 4 (1994). *Acta Cryst.* D**50**, 760–763.

Crull, G. B. & Goff, H. M. (1993). *J. Inorg. Biochem.* **15**, 181–182.

Danishefsky, A. T., Housset, D., Kim, K. S., Tao, F., Fuchs, J., Woodward, C. & Wlodawer, A. (1993). *Protein Sci.* **2**, 577–587.

Ducruix, A., Guilloteau, J. P., Riès-Kautt, M. & Tardieu, A. (1996). *J. Cryst. Growth*, **168**, 28–39.

Eigenbrot, C., Randal, M. & Kossiakoff, A. A. (1990). *Protein Eng.* **3**, 591–598.

Eigenbrot, C., Randal, M. & Kossiakoff, A. A. (1992). *Protein Struct. Funct.* **14**, 75–87.

Fourme, R., Dhez, P., Benoit, J. P., Kahn, R., Dubuisson, J. M., Besson, P. & Frouin, J. (1992). *Rev. Sci. Instrum.* **63**, 982–987.

French, S. & Wilson, K. (1978). *Acta Cryst.* A**34**, 517–525.

Galanter, W. L. & Labotka, R. J. (1991). *Biochim. Biophys. Acta*, **1079**, 146–151.

Hamiaux, C. (1998). Unpublished results.

Housset, D., Kim, K. S., Fuchs, J., Woodward, C. & Wlodawer, A. (1991). *J. Mol. Biol.* **220**, 757–770.

Howell, P. L. (1995). *Acta Cryst.* D**51**, 654–662.

Howell, P. L., Almo, S. C., Parsons, M. R., Hadju, J. & Petsko, G. A. (1992). *Acta Cryst.* B**48**, 200–207.
Janin, J. & Rodier, F. (1995). *Protein Struct. Funct. Genet.* **23**, 580–587.
Jolivalt, C., Böckmann, A., Riès-Kautt, M., Ducruix, A. & Guittet, E. (1998). *Biophys. Chem.* **71**, 221–234.
Jolivalt, C., Riès-Kautt, M., Chevallier, P. & Ducruix, A. (1997). *J. Synchrotron Rad.* **4**, 28–35.
Jones, T. A., Zou, J. Y., Cowan, S. W. & Kjeldgaard, M. (1991). *Acta Cryst.* A**47**, 110–119.
Kassel, B. (1970). *Methods Enzymol.* **19**, 844–852.
Lafont, S. (1997). Thèse de Doctorat, Université d'Aix-Marseille III, France. (Order No. 96AIX30047.)
Lafont, S., Veesler, S., Astier, J. P. & Boistelle, R. (1997). *J. Cryst. Growth*, **173**, 132–140.
Leslie, A. (1994). *MOSFLM User Guide, MOSFLM version 5.20*. MRC Laboratory of Molecular Biology, Cambridge, United Kingdom.
Low, B. (1992). Personal communication.
Luzzati, V. (1952). *Acta Cryst.* **5**, 802–810.
Marquart, M., Walter, J., Deisenhofer, J., Bode, W. & Huber, R. (1983). *Acta Cryst.* B**39**, 480–490.
Modi, S., Behere, D. V. & Mitra, S. (1989*a*). *J. Biol. Chem.* **264**, 19677–19684.
Modi, S., Behere, D. V. & Mitra, S. (1989*b*). *Biochemistry*, **28**, 4689–4694.
Navaza, J. (1994). *Acta Cryst.* D**50**, 157–163.
Navaza, J., Mauguen, Y., Saludjian, P., Prangé, T., Alzari, P. & Bentley, G. (1993). *Acta Cryst.* A**49**(S), C49.
Otting, G. & Wütrich, K. (1989). *J. Am. Chem. Soc.* **111**, 1871–1875.
Parkin, S., Rupp, B. & Hope, H. (1996). *Acta Cryst.* D**52**, 18–29.
Ramakrishnan, C. & Ramachandran, G. N. (1965). *Biophys. J.* **5**, 909–933.
Riès-Kautt, M. & Ducruix, A. (1989). *J. Biol. Chem.* **264**, 745–748.
Riès-Kautt, M. & Ducruix, A. (1991). *J. Cryst. Growth*, **110**, 20–25.
Riès-Kautt, M., Ducruix, A. & Van Dorsselaer, A. (1994). *Acta Cryst.* D**50**, 366–369.
Rossmann, M. G., Leslie, A. G. W., Abdel-Meguid, S. S. & Tsukihara, T. (1979). *J. Appl. Cryst.* **12**, 570–581.
Saludjian, P., Prangé, T., Navaza, J., Menez, R., Guilloteau, J. P., Riès-Kautt, M. & Ducruix, A. (1992). *Acta Cryst.* B**48**, 520–531.
Smith, J. L., Corfield, P. W. R., Hendrickson, W. A. & Low, B. (1988). *Acta Cryst.* A**44**, 357–368.
Tchertanov, L. & Pascard, C. (1997). *Acta Cryst.* B**53**, 904–915.
Veesler, S., Lafont, S., Marcq, S., Astier, J. P. & Boistelle, R. (1996). *J. Cryst. Growth*, **168**, 124–129.
Wilson, A. J. C. (1949). *Acta Cryst.* **2**, 318–321.
Winkler, F. K., Schutt, C. E. & Harrison, S. C. (1979). *Acta Cryst.* A**35**, 901–911.
Wlodawer, A., Deisenhofer, J. & Huber, R. (1987). *J. Mol. Biol.* **193**, 145–156.
Wlodawer, A., Nachman, J. Gilliland, G. L. Gallagher, W. & Woodward, C. (1987). *J. Mol. Biol.* **198**, 469–480.
Wlodawer, A., Walter, J., Huber, R. & Sjölin, L. (1984). *J. Mol. Biol.* **180**, 301–329.